Inorganic Chemistry
Article

Inorg. Chem. **2010**, *49*, 1355–1362 **1355**
DOI: 10.1021/ic9011586

Electronic Structure and Circular Dichroism of Tris(bipyridyl) Metal Complexes within Density Functional Theory

Jing Fan,[†] Jochen Autschbach,[‡] and Tom Ziegler*[,†]

[†]*Department of Chemistry, University of Calgary, 2500 University Drive, Calgary, Alberta, Canada T2N 1N4, and* [‡]*Department of Chemistry, University at Buffalo, State University of New York, 312 Natural Science Complexes, Buffalo, New York 14260-30000*

Received June 16, 2009

Time-dependent density functional theory (TD-DFT) has been employed to calculate the electronic circular dichroism (CD) spectra of tris-bidentate iron group complexes $[M(L-L)_3]^{2+}$ (M = Fe, Ru, Os; L−L = 2,2′-bipyridine). The simulated CD spectra are compared with the experiment, and reasonably good agreement is obtained. In this study, much effort has been made to interpret the exciton CD arising from the long-axis-polarized $\pi \rightarrow \pi^*$ excitations in the ligands of the complexes. Metal−ligand orbital interactions as well as the origin of the optical activity of the exciton transitions have been elucidated in connection with the detailed analysis of the TD-DFT results within a general model that is applicable to similar chiral compounds.

1. Introduction

Electronic circular dichroism (CD), the difference in absorption between left and right circularly polarized light, has become one of the most popular chiroptical methods for the elucidation of electronic structures, the assignment of transitions, and the determination of the absolute configuration of chiral molecules.[1−4] Because no direct spectroscopic method such as X-ray crystallography is readily available for the determination of molecular structures in solution or in the gas phase, chiroptical methods are often the only means by which to determine absolute configurations of chiral coordination compounds.

Tris- or bis-bidentate complexes containing conjugated ligands, typically bipyridine (bpy) and phenanthroline (phen), exhibit intense CD in the UV absorption region that is ascribed to ligand-centered (LC) transitions of the conjugated ligands. However, for complexes containing only one of the conjugated ligands, e.g., $[Co(en)_2phen]^{3+}$, the CD in the same absorption region was found[5] to be extremely weak. The intense CD bands in the tris- or bis-bidentate complexes were rationalized in terms of Coulombic coupling of the $\pi \rightarrow \pi^*$ transitions in the individual ligands. This is referred to as exciton theory, which was first proposed by Kuhn et al.[6,7] and later applied by Mason et al.[8,9] and Bosnich[10,11] to bpy and phen complexes. According to the exciton model, the CD arising from long-axis-polarized LC transitions will appear strongly positive at lower energies and strongly negative at higher energies if the molecule has the Λ absolute configuration. The theory has thus been used nonempirically for the determination of the absolute configuration of the coordination compounds. Ziegler and von Zelewsky recently demonstrated the application of this model to complexes with the chiragen ligand family.[12]

On the other hand, the metal-to-ligand charge-transfer (MLCT) transitions in the visible region of the metal, especially ruthenium(II), polypyridyl, and related complexes, have attracted much interest because of the properties of the MLCT excited states and their proposed applications in a wide range of areas such as photosensitizers in solar cells,[13−15] photoprobes and photoreagents for biomolecules,[16−19] and light-emitting devices.[20−22]

*To whom correspondence should be addressed. E-mail: ziegler@ucalgary.ca.

(1) Velluz, L.; Legrand, A.; Grosjean, M. *Optical circular dichroism: principles, measurements, and applications*; VCH: New York, 1969.
(2) Charney, E. *The molecular basis of optical activity*; John Wiley & Sons Ltd.: New York, 1979.
(3) Rodger, A. *Circular dichroism and linear dichroism*; Oxford University Press, Oxford, U.K., 1997.
(4) Berova, N., Nakanishi, K., Woody, R. W., Eds. *Circular Dichroism: Principles and Applications*; VCH: New York, 2000.
(5) Hidaka, J.; Douglas, B. E. *Inorg. Chem.* **1964**, *3*, 1180–1184.
(6) Kuhn, W. Z. *Phys. Chem.* **1929**, *B4*, 14.
(7) Kuhn, W.; Bein, K. *Z. Phys. Chem., Abt. B* **1934**, 335.
(8) Mason, S. F. *Inorg. Chim. Acta* **1968**, 89–109.
(9) McCaffery, A. J.; Mason, S. F.; Norman, B. J. *J. Chem. Soc. A* **1969**, 1428–1441.
(10) Bosnich, B. *Acc. Chem. Res.* **1969**, 266–273.
(11) Bosnich, B. *Inorg. Chem.* **1968**, *7*, 2379–2386.
(12) Ziegler, M.; von Zelewsky, A. *Coord. Chem. Rev.* **1998**, *177*, 257–300.
(13) Hagfeldt, A.; Grätzel, M. *Chem. Rev.* **1995**, *95*, 49–68.
(14) Altobello, S.; Argazzi, R.; Caramori, S.; Contado, C.; Da Fre, S.; Rubino, P.; Chone, C.; Larramona, G.; Bignozzi, C. A. *J. Am. Chem. Soc.* **2005**, *127*, 15342–15343.
(15) Koops, S. E.; O'Regan, B. C.; Barnes, P. R. F.; Durrant, J. R. *J. Am. Chem. Soc.* **2009**, *131*, 4808–4818.
(16) Kelly, J. M.; Tossi, A. B.; McConnell, D. J.; OhUigin, C. *Nucleic Acids Res.* **1985**, *13*, 6017–6034.

Published on Web 01/21/2010

In this context, theoretical investigations on the photoabsorption properties of these compounds would be worthwhile from both the theoretical and practical points of view. Nevertheless, almost all of the early studies have focused on the absorption properties of charge-transfer transitions of the relevant complexes,[23−28] whereas theoretical studies of the CD spectra are rather sparse.[29−34] In this paper, we study the electronic CD spectra over the whole experimentally accessible range for the model compounds using time-dependent density functional theory (TD-DFT).[35−38] The DFT method, because of its accuracy and computational efficiency, has in recent years become a popular approach for calculation of the optical activity. It has been applied to calculate the CD spectra of a number of transition-metal complexes,[34,39−49] including the work on $[M(phen)_3]^{2+}$ (M = Fe, Ru, Os) by Autschbach et al.[34] It is our purpose here to give a detailed analysis for the $[M(bpy)_3]^{2+}$ (M = Fe, Ru, Os) complexes. We hope by the present work to obtain a relationship between the CD spectra of the $[M(bpy)_3]^{2+}$ complexes and their geometric and electronic structures. We will further compare our results of $[M(bpy)_3]^{2+}$ to those of the previously studied $[M(phen)_3]^{2+}$.

The term "exciton" is used throughout this work to characterize all LC $\pi \rightarrow \pi^*$ excitations. We might thus be using this term more broadly than in the classical exciton theory.

2. Computational Details

The calculations reported in this paper are carried out with a modified version of the Amsterdam Density Functional (ADF) package.[50] The CD version by Autschbach et al.[51−53] is an extension of the TD-DFT in ADF developed by van Gisbergen, Baerends, and co-workers.[54−56] We have used the valence triple-ζ doubly polarized (TZ2P) Slater basis sets for the metals and the valence triple-ζ polarized (TZP) orbitals for carbon, nitrogen, and hydrogen. In all calculations, the inner shell cores (1s on C and N and up to 2p, 3d, and 4f for Fe, Ru, and Os, respectively) have been considered to be frozen. Rotatory strengths were calculated by the dipole-length formula. Rotatory strengths computed with this formula are in good agreement with those obtained from the dipole-velocity form. The 50 lowest-spin and symmetry-allowed excitations were calculated for each complex. On the basis of the computed singlet excitation energies, associated oscillator, and rotatory strengths, the CD spectra have been simulated and compared with experimental data. A reasonable overall agreement with the experiment was obtained by choosing a Gaussian half-width parameter σ of 0.13 eV for all of the simulated spectra. We should note that the bandwidth is chosen here as an adjustable parameter in order to mimic a real spectrum. We do not calculate band shapes from first principles. Numerical data for the experimental spectra have been extracted using *g3data* software.[57]

Relativistic effects were taken into account by a scalar zero-order regular approximation approach. All TD-DFT calculations are based on optimized geometries in D_3 symmetry. The Vosko−Wilk−Nusair[58] local density approximation (LDA) with the Becke88−Perdew86 (BP86) gradient corrections[59,60] has been used in all of the calculations. Geometries optimized by BP86 reproduce experimental structures well for the complexes considered here. Thus, bond distances are reproduced by 0.02 Å and bond angles by 1°. The adiabatic LDA kernel has been employed for the frequency-dependent linear response of the molecular potential. Experience has shown that excited states lying well below the Kohn−Sham continuum can be properly described within the adiabatic approximation.[61−63] The present work is restricted to vertical

(17) Fleisher, M. B.; Waterman, K. C.; Turro, N. J.; Barton, J. K. *Inorg. Chem.* **1986**, *25*, 3549–3551.
(18) Elias, B.; Mesmaeker, A. K. *Coord. Chem. Rev.* **2006**, *250*, 1627–1641.
(19) Moucheron, C. *New J. Chem.* **2009**, *33*, 235–245.
(20) Baldo, M. A.; O'Brien, D. F.; You, Y.; Shoustikov, A.; Sibley, S.; Thompson, M. E.; Forrest, S. R. *Nature* **1998**, *395*, 151–154.
(21) Buda, M.; Kalyuzhny, G.; Bard, A. J. *J. Am. Chem. Soc.* **2002**, *124*, 6090–6098.
(22) Pentlehner, D.; Grau, I.; Yersin, H. *Chem. Phys. Lett.* **2008**, *455*, 72–78.
(23) Bossert, J.; Daniel, C. *Coord. Chem. Rev.* **2008**, *252*, 2493–2503.
(24) Alary, F.; Boggio-Pasqua, M.; Heully, J.; Marsden, C. J.; Vicendo, P. *Inorg. Chem.* **2008**, *47*, 5259–5266.
(25) Kitao, O.; Sugihara, H. *Inorg. Chim. Acta* **2008**, *361*, 712–728.
(26) Kober, E. M.; Meyer, T. J. *Inorg. Chem.* **1982**, *21*, 3967–3977.
(27) Blomquist, J.; Nordén, B.; Sundbom, M. *Theor. Chim. Acta* **1973**, *28*, 313–337.
(28) Day, P.; Sanders, N. *J. Chem. Soc. A* **1967**, 1536–1541.
(29) Niezborala, C.; Hache, F. *J. Phys. Chem. A* **2007**, *111*, 7732–7735.
(30) Daul, C.; Schlaepfer, C. W. *J. Chem. Soc., Dalton Trans.* **1988**, 393–400.
(31) Sanders, N. *J. Chem. Soc., Dalton Trans.* **1972**, 345–350.
(32) Sanders, N. *J. Chem. Soc. A* **1971**, 1563–1569.
(33) Hanazaki, I.; Nagakura, S. *Inorg. Chem.* **1969**, *8*, 654–662.
(34) Le Guennic, B.; Hieringer, W.; Görling, A.; Autschbach, J. *J. Phys. Chem. A* **2005**, *109*, 4836–4846.
(35) Runge, E.; Gross, E. K. U. *Phys. Rev. Lett.* **1984**, *52*, 997–1000.
(36) Casida, M. E. Time-dependent density functional response theory for molecules. In *Recent advances in density functional methods*; Chong, D. P., Ed.; World Scientific: Singapore, 1995.
(37) Gross, E. K. U.; Dobson, J. F.; Petersilka, M. In *Density Functional Theory*; Nalewajski, R. F., Ed.; Springer: Heidelberg, Germany, 1996.
(38) Marques, M.; Ullrich, C. A.; Nogueira, F.; Rubio, A.; Burke, K.; Gross, E. K. U. *Time-dependent Density Functional Theory*; Springer: Heidelberg, Germany, 2006.
(39) Jorge, F. E.; Autschbach, J.; Ziegler, T. *Inorg. Chem.* **2003**, *42*, 8902–8910.
(40) Diedrich, C.; Grimme, S. *J. Phys. Chem. A* **2003**, *107*, 2524–2539.
(41) Vargas, A.; Zerara, M.; Krausz, E.; Hauser, A.; Lawson Daku, L. M. *J. Chem. Theor. Comput.* **2006**, *2*, 1342–1359.
(42) Thulstrup, P. W.; Larsen, E. *Dalton Trans.* **2006**, *14*, 1784–1789.
(43) Autschbach, J.; Jorge, F. E.; Ziegler, T. *Inorg. Chem.* **2003**, *42*, 2867–2877.
(44) Bark, T.; von Zelewsky, A.; Rappoport, D.; Neuburger, M.; Schaffner, S.; Lacour, J.; Jodry, J. *Chem.—Eur. J.* **2004**, *10*, 4839–4845.
(45) Jorge, F. E.; Autschbach, J.; Ziegler, T. *J. Am. Chem. Soc.* **2005**, *127*, 975–985.
(46) Fan, J.; Ziegler, T. *Inorg. Chem.* **2008**, *47*, 4762–4773.
(47) Fan, J.; Seth, M.; Autschbach, J.; Ziegler, T. *Inorg. Chem.* **2008**, *47*, 11656–11668.
(48) Coughlin, F. J.; Westrol, M. S.; Oyler, K. D.; Byrne, N.; Kraml, C.; Zysman-Colman, E.; Lowry, M. S.; Bernhard, S. *Inorg. Chem.* **2008**, *47*, 2039–2048.
(49) Coughlin, F. J.; Oyler, K. D.; Pascal, R. A., Jr.; Bernhard, S. *Inorg. Chem.* **2008**, *47*, 974–979.
(50) *Amsterdam Density Functional program, Theoretical Chemistry*; Vrije Universiteit: Amsterdam, The Netherlands, **2009**; URL http://www.scm.com.
(51) Autschbach, J.; Ziegler, T.; van Gisbergen, S. J. A.; Baerends, E. J. *J. Chem. Phys.* **2002**, *116*, 6930–6940.
(52) Autschbach, J.; Ziegler, T. *J. Chem. Phys.* **2002**, *116*, 891–896.
(53) Autschbach, J.; Ziegler, T.; Patchkovskii, S.; van Gisbergen, S. J. A.; Baerends, E. J. *J. Chem. Phys.* **2002**, *117*, 581–592.
(54) van Gisbergen, S. J. A.; Snijders, J. G.; Baerends, E. J. *J. Chem. Phys.* **1995**, *103*, 9347–9354.
(55) van Gisbergen, S. J. A.; Snijders, J. G.; Baerends, E. *J. Comput. Phys. Commun.* **1999**, *118*, 119–138.
(56) van Gisbergen, S. J. A.; Fonseca-Guerra, C.; Baerends, E. J. *J. Comput. Chem.* **2000**, *21*, 1511–1523.
(57) Frantz, J. *g3data*; **2002**, URL http://www.frantz.fi/software/g3data.php.
(58) Vosko, S. H.; Wilk, L.; Nusair, M. *Can. J. Phys.* **1980**, *58*, 1200–1211.
(59) Becke, A. D. *Phys. Rev. A* **1988**, *38*, 3098–3100.
(60) Perdew, J. P. *Phys. Rev. B* **1986**, *33*, 8822–8824.
(61) Bauernschmitt, R.; Ahlrichs, R. *Chem. Phys. Lett.* **1996**, *256*, 454.
(62) Casida, M. E.; Jamorski, C.; Casida, K. C.; Salahub, D. R. *J. Chem. Phys.* **1998**, *108*, 4439.
(63) Furche, F.; Ahlrichs, R.; Wachsmann, C.; Weber, E.; Sobanski, A.; Vögtle, F.; Grimme, S. *J. Am. Chem. Soc.* **2000**, *122*, 1717–1724.

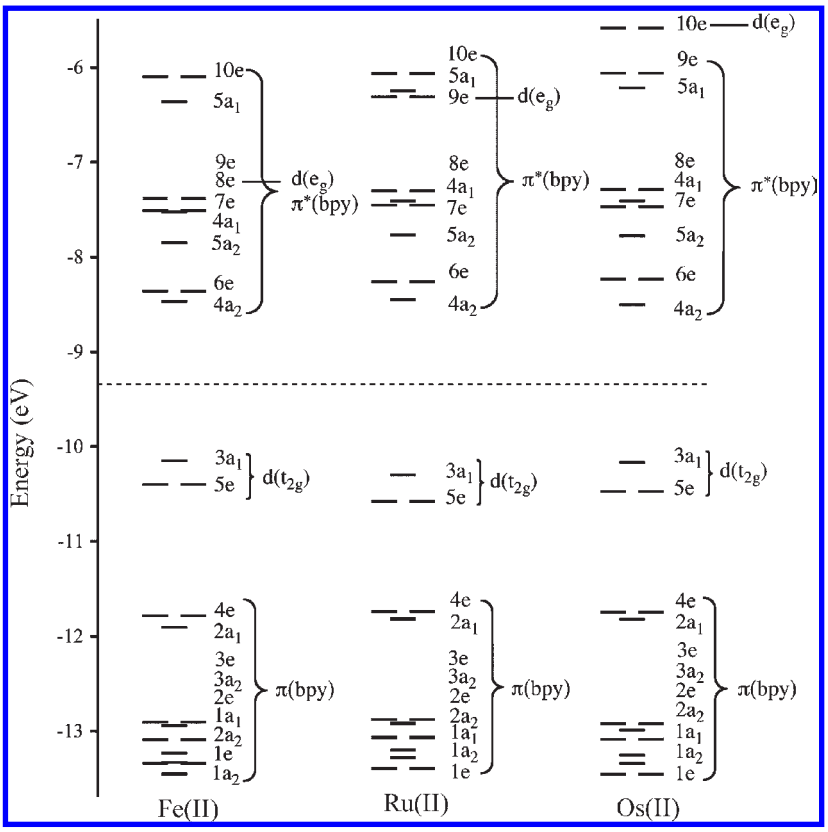

Figure 1. Molecular level diagrams for $[M(bpy)_3]^{2+}$ complexes. The orbitals below the dotted line are occupied.

excitations. Vibrational effects have been neglected because we expect them to be small for rigid coordinated molecules like the tris-bidentate complex ions studied here.

3. Results and Discussion

In this section, results from DFT calculations on the CD spectra and the electronic structure of the tris(bipyridyl) complexes are presented. The simulated CD spectra are compared to experimental findings[8] where such data are available. CD bands in the experimental and simulated spectra are in the following marked by Roman numerals and alphabetic letters, respectively. For each system, the positions of the computed excitation energies as well as the sign and magnitude of the rotatory strengths are indicated by a bar spectrum. Transitions that have the most important contributions to a given CD spectrum are labeled with Arabic numerals and discussed in detail later. In different complexes, transitions due to equivalent one-electron excitations carry the same numbering in order to facilitate a comparison between complexes. The results of the analogous phen complexes are included in the Supporting Information. Comparisons are also made between bpy and phen systems.

3.1. $[M(bpy)_3]^{2+}$. Figure 1 displays the molecular orbital (MO) diagrams for all three bipyridyl complexes with M = Fe, Ru, and Os. We see that the diagrams resemble each other quite closely. In all three complexes, the highest occupied MOs (HOMOs; $3a_1$ and 5e) are invariably the $t_{2g}(d\pi)$ set of the metal d orbitals that split into the a_1 and e representations under D_3 symmetry (see Figure S1 in the Supporting Information). The occupied orbitals shown below the HOMOs have a dominant ligand π character. They are made up of occupied π orbitals in a free bpy ligand transforming as a_2 or b_1 in a free planar bpy ligand of C_{2v} symmetry (see Figure S2 in the Supporting Information). Symmetry combinations of the a_2 ligand orbitals transform as a_1 and e under D_3 symmetry, whereas the b_1 symmetry combinations transform as a_2 and e. The symmetry ligand orbitals are shown in Table S1 in the Supporting Information. The dominant contribution to the occupied MOs 4e and $2a_1$ is the highest occupied π orbital of bpy, shown as $2a_2$ in Figure 2. The lowest uoccupied MOs (LUMOs; $4a_2$ and 6e) and the orbitals above are ligand-based π^* orbitals, except for the ones labeled 8e in iron, 9e in ruthenium, and 10e in osmium, which represent the metal dσ-based e_g set. We note, as expected, an increment in the $t_{2g}-e_g$ crystal-field splitting in going from iron to osmium. The LUMOs ($4a_2$ and 6e) are made up of combinations of π^* orbitals (β_i^{π}; i = 1, 3), where each β_i^{π} transforms as b_1 under C_{2v} symmetry (Table S1 in the Supporting Information). The dominant contribution from each bpy ligand comes from the lowest unoccupied orbital shown in Figure 2 as $1b_1$.

The most important MOs for the interpretation of the CD spectra are the HOMO$-$1's ($2a_1$ and 4e), the HOMOs (5e and $3a_1$), and the LUMOs ($4a_2$ and 6e) of Figure 1. It is noted that the character as well as the trigonal splitting pattern of the HOMO$-$1's, the HOMOs, and the LUMOs is in line with the prediction made by Mason based on Hückel calculations[8] for all three metals and by Daul et al. on multiple scattering X_α (MSX_α) and Hückel models[30] for the ruthenium and osmium systems. In the iron analogous, however, the LUMOs were determined[30] to be the metal e_g set rather than π^* ligand orbitals as found here. Moreover, the authors found that the mixing between the occupied metal t_{2g} orbitals and the empty π^* orbitals of the ligands was dominant, while the mixing

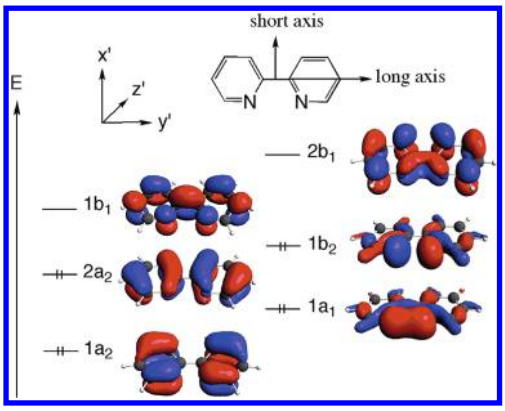

Figure 2. Frontier MOs in free bpy (C_{2v}).

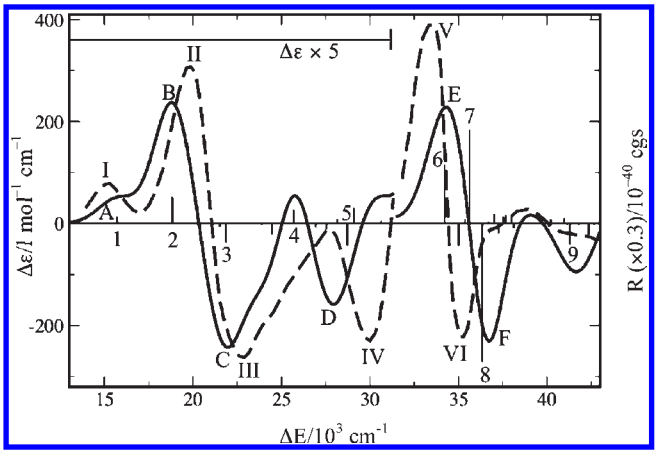

Figure 3. Simulated (solid line) and experimental[8] (dashed line) CD spectra for Λ-$[Os(bpy)_3]^{2+}$. The computed excitations are blue-shifted by 2.0×10^3 cm^{-1}. The low-energy parts of both spectra are magnified by a factor of 5. Theoretical excitation energies and rotatory strengths are indicated by bars. The factor by which computed rotatory strengths are scaled is indicated in parentheses of the right-hand scale.

between the t_{2g} orbitals and the occupied π orbitals was significantly smaller. We find from our DFT calculations, however, that the t_{2g} orbitals interact comparably with both the occupied π and empty π^* orbitals. We see for all three metals that the trigonal splitting of the metal t_{2g} levels places $3a_1$ above 5e (see Figure 1). This splitting is determined by the interaction between $d\pi$ and linear symmetry combinations of $\pi(2a_2)$ or $\pi^*(1b_1)$ on the bpy ligands. The interaction between $d\pi$ and $\pi^*(1b_1)$ is stabilizing as $\pi^*(1b_1)$ is empty. However, the D_3 symmetry combinations of $\pi^*(1b_1)$ transform as e and a_2. Thus, the $d\pi(e)$ component 5e is stabilized while the $d\pi(a_1)$ component $3a_1$ is unperturbed because of the lack of interaction between $d\pi$ and $\pi^*(1b_1)$. On the other hand, the same interaction leaves 6e above $4a_2$ in energy as only the e component of $\pi^*(1b_1)$ is destabilized whereas the a_2 combination is unperturbed.

While the interaction between $d\pi$ and $\pi^*(1b_1)$ accounts for the LUMO splitting $6e > 4a_2$, it is only one of the factors responsible for the $d\pi$ splitting $3a_1 > 5e$. The second factor is the interaction between $d\pi$ and $\pi(2a_2)$. This interaction is destabilizing as $\pi(2a_2)$ is occupied. Further, the symmetry combinations of $\pi(2a_2)$ transform as a_1 and e, so that both $d\pi(e)$ and $d\pi(a_1)$ are destabilized. However, as shown elsewhere by symmetry considerations,[46] the overlap

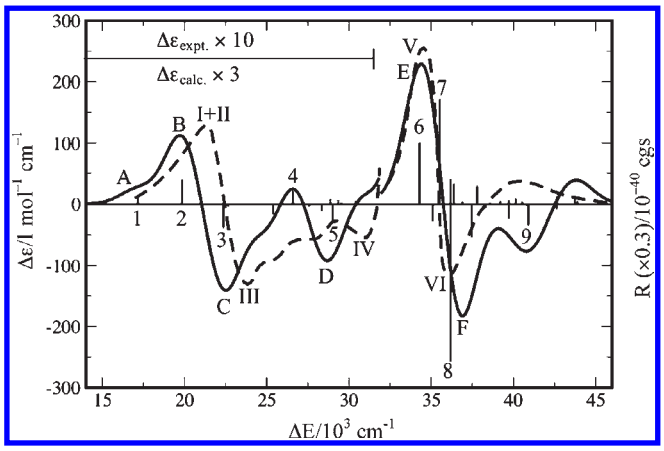

Figure 4. Simulated (solid line) and experimental[8] (dashed line) CD spectra for Λ-$[Ru(bpy)_3]^{2+}$. The computed excitations are blue-shifted by 2.0×10^3 cm^{-1}. The low-energy part of the theoretical (experimental) spectrum is magnified by a factor of 3 (10). See also the caption for Figure 3.

between a_1 and $d\pi(a_1)$ is twice as large in absolute terms as that between e and $d\pi(e)$. The interaction between $d\pi$ and $\pi(2a_2)$ will, as a consequence, add to the destabilization of 5e compared to $3a_1$ and place the ligand-based MO $2a_1$ below 4e. We note that the trigonal splittings $3a_1 > 5e$ and $6e > 4a_2$ increase through the series M = Fe, Ru, and Os as the metal−ligand orbital overlap increases in absolute terms. In fact, we find for the $6e-4a_2$ separations 0.10 eV (Fe), 0.19 eV (Ru), and 0.26 eV (Os). The trigonal splitting will play an important role in the assignment of the CD spectra for $[M(bpy)_3]^{2+}$. We shall before we proceed with our assignment point out that the σ-type orbitals on the bpy ligands give rise to a number of symmetry combinations, as shown in Table S1 in the Supporting Information. One of these combinations involves the $\sigma(e)$ orbitals. The interaction between $\sigma(e)$ and $d\sigma(e)$ has a major contribution to the $d\sigma-d\pi$ crystal-field splitting.

Figures 3−5 compare simulated and experimental CD spectra. The relevant spectral information has been compiled in Tables 1−3. The agreement between theory and experiment is good, especially for the ruthenium and osmium systems. In all three spectra, the lower-energy part ($< 30 \times 10^3$ cm^{-1}) is ascribed, both theoretically and experimentally,[8,26−28,31−33] to MLCT transitions. Of the MLCT transitions from the metal t_{2g} levels to the LUMOs of Figure 1, the three 1(A_2), 2(E), and 3(E) are shown to have considerable CD intensities. The three transitions are largely due to the $3a_1 \rightarrow 4a_2$, $5e \rightarrow 4a_2$, and $5e \rightarrow 6e$ one-electron excitations, respectively. The excitations give rise to bands A−C in the simulated CD spectra of the ruthenium and osmium complexes after a blue shift of 2×10^3 cm^{-1}. They are assigned to bands I−III of the experimental spectra (Figures 3 and 4). The simulated spectrum for the iron system is very similar to those of the heavier elements ruthenium and osmium in the low-energy region. The only difference is that the excitations for M = Fe are calculated to take place at lower energies. In fact, the calculated bands A and B for iron are predicted to be situated at frequencies not explored experimentally. We denote for this reason the first observed band as III and assign it to the simulated band C. On the other hand, we assign the simulated bands A and B to two yet unobserved

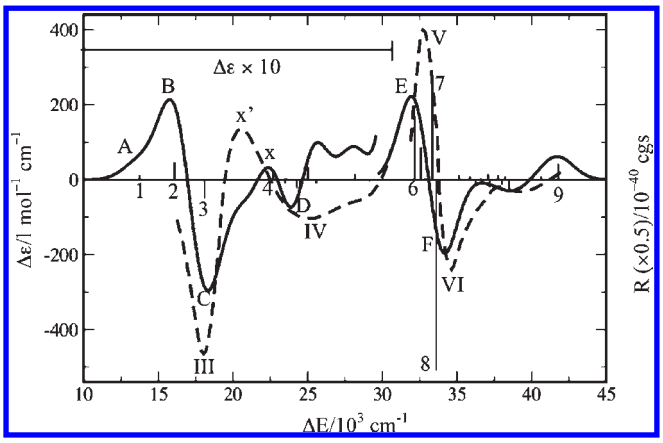

Figure 5. Simulated (solid line) and experimental[8] (dashed line) CD spectra for Λ-$[Fe(bpy)_3]^{2+}$. The low-energy parts of both spectra are magnified by a factor of 10. See also the caption for Figure 3. The numbering of the experimental spectrum starts with III to undertake the similarity with that for M = Ru, and Os. It is assumed that I and II are at lower energy than those recorded in ref 8.

Table 1. Calculated Excitation Energies and Rotatory Strengths for Λ-$[Os(bpy)_3]^{2+}$

				one-electron excitation[d]	
no.	R^a (10^{-40} cgs)	ΔE^b (10^3 cm^{-1})	symmetry[c]	MO → MO	%
1	+43.31	13.73	A_2	$3a_1 \rightarrow 4a_2$	100
2	+175.92	16.82	E	$5e \rightarrow 4a_2$	87
3	−125.31	19.87	E	$5e \rightarrow 6e$	83
4	+86.14	23.69	E	$3a_1 \rightarrow 8e$	78
				$5e \rightarrow 7e$	11
5	−142.26	26.72	E	$4e \rightarrow 4a_2$	43
				$5e \rightarrow 8e$	34
6	+384.46	32.22	E	$4e \rightarrow 5a_2$	67
				$2a_1 \rightarrow 6e$	12
7	+612.84	33.64	E	$2a_1 \rightarrow 6e$	20
				$4e \rightarrow 5a_2$	18
				$4e \rightarrow 6e$	16
				$4e \rightarrow 7e$	13
				$5e \rightarrow 5a_1$	12
8	−906.83	34.36	A_2	$4e \rightarrow 6e$	43
				$4e \rightarrow 7e$	21
				$2a_1 \rightarrow 4a_2$	16
9	−136.31	39.30	E	$1a_1 \rightarrow 6e$	20
				$3e \rightarrow 6e$	15
				$2a_1 \rightarrow 8e$	13
				$3a_2 \rightarrow 6e$	13

[a] Rotatory strength; for the degenerate E states, the rotatory strength given is the sum of the contributions from E_x and E_y. [b] Excitation energy. [c] Symmetry of the excited state. [d] Major contributions from one-electron excitations to the transition.

bands (I + II) in the unexplored region below 16.0 × 10^3 cm^{-1}. It is interesting to note that semiempirical calculations[27] also predicted two spin-allowed MLCT transitions in this region. Alternatively, the disagreement of the CD results in this region might be due to a reduced efficiency of the nonhybrid functional when it is applied to the 3d metals.[34] This issue will be examined in a later study. The emphasis of the present work is on the interpretation and analysis of the origin of the exciton CD. The simulation of the exciton CD seems not to differ much whether or not use is made of pure or hybrid DFT functionals.[34] Thus, any problems one might find with the MLCT transitions below 15 × 10^3 cm^{-1} in the iron complexes are of little consequence for the main objective in the current work.

Table 2. Calculated Excitation Energies and Rotatory Strengths for Λ-$[Ru(bpy)_3]^{2+a}$

				one-electron excitation	
no.	R (10^{-40} cgs)	ΔE (10^3 cm^{-1})	symmetry	MO → MO	%
1	+32.74	15.16	A_2	$3a_1 \rightarrow 4a_2$	100
2	+134.14	17.85	E	$5e \rightarrow 4a_2$	89
3	−129.76	20.36	E	$5e \rightarrow 6e$	85
4	+68.99	24.58	E	$3a_1 \rightarrow 8e$	81
				$5e \rightarrow 7e$	10
5	−90.15	27.02	E	$4e \rightarrow 4a_2$	62
				$5e \rightarrow 8e$	13
6	+334.98	32.29	E	$4e \rightarrow 5a_2$	69
				$2a_1 \rightarrow 6e$	11
7	+571.72	33.52	E	$2a_1 \rightarrow 6e$	21
				$4e \rightarrow 5a_2$	17
				$4e \rightarrow 6e$	16
				$4e \rightarrow 7e$	14
				$4e \rightarrow 4a_2$	11
8	−860.19	34.19	A_2	$4e \rightarrow 6e$	45
				$2a_1 \rightarrow 4a_2$	19
				$4e \rightarrow 7e$	14
9	−117.83	38.90	E	$1a_1 \rightarrow 6e$	20
				$2a_1 \rightarrow 8e$	13
				$3e \rightarrow 6e$	12

[a] For a description of each column, see the footnotes in Table 1.

Table 3. Calculated Excitation Energies and Rotatory Strengths for Λ-$[Fe(bpy)_3]^{2+a}$

				one-electron excitation	
no.	R (10^{-40} cgs)	ΔE (10^3 cm^{-1})	symmetry	MO → MO	%
1	+21.47	13.74	A_2	$3a_1 \rightarrow 4a_2$	100
2	+93.52	16.08	E	$5e \rightarrow 4a_2$	89
				$5e \rightarrow 6e$	10
3	−100.60	18.09	E	$5e \rightarrow 6e$	85
4	+44.84	22.69	E	$3a_1 \rightarrow 9e$	58
				$3a_1 \rightarrow 8e$	21
				$5e \rightarrow 4a_1$	10
6	+338.90	32.14	E	$4e \rightarrow 5a_2$	69
				$2a_1 \rightarrow 6e$	11
7	+556.58	33.35	E	$5e \rightarrow 5a_1$	32
				$2a_1 \rightarrow 6e$	16
				$4e \rightarrow 7e$	14
				$4e \rightarrow 6e$	11
8	−1019.80	33.61	A_2	$4e \rightarrow 6e$	47
				$2a_1 \rightarrow 4a_2$	28
9	−57.31	38.50	E	$1a_1 \rightarrow 6e$	27
				$2a_1 \rightarrow 7e$	13
				$2a_1 \rightarrow 9e$	12
				$3e \rightarrow 7e$	12

[a] For a description of each column, see the footnotes in Table 1.

The CD bands at about 35 × 10^3 cm^{-1} are assigned to the exciton excitations centered on the bpy ligands. We shall shortly show that these excitations are polarized in the plane of the ligand molecule along an axis connecting the two N atoms. A satisfactory agreement between the theory and experiment is obtained in this region for all three complexes. The two CD bands have opposite signs, with the positive one occurring at lower energy, in agreement with the experimental CD spectra of the Λ enantiomer.

3.2. Comparison between $[M(bpy)_3]^{2+}$ and $[M(phen)_3]^{2+}$. The MO diagrams as well as the main features of the CD spectra for the three phen complexes (Figures S3 and S5−S7 in the Supporting Information) display a close resemblance to those of the analogous bpy systems as a whole. The band assignments are basically the same for the two ligand systems; the lower-energy part of the spectra

arises from the MLCT transitions, while the higher-energy part is due to LC exciton transitions. In general, the CD spectra of the phen complexes exhibit a higher energy of $(0.5-1) \times 10^3$ cm^{-1} for the CT region and about 2×10^3 cm^{-1} for the exciton region compared to those in the bipyridyl counterparts. Detailed information of the CD calculations for $[M(phen)_3]^{2+}$ indicates a significant involvement of the ligand-based LUMOs and HOMO−2's (instead of the HOMO−1's due to the symmetry constraints) in the exciton region and the LUMO+1's, LUMO+2's, and metal-based HOMOs in the MLCT region.

It is noted that the band at about 25×10^3 cm^{-1} of the simulated spectrum for $[Fe(phen)_3]^{2+}$ is due to an almost pure d−d transition. The band that is quite unique for this metal is labeled x, and it is assigned to band x′ of the experimental spectrum (Figure S7 in the Supporting Information). The relatively high CD intensity of the d−d transitions can be ascribed to metal−ligand (antibonding) orbital interactions that result in (out-of-phase) mixing of ligand π and/or σ orbitals into the d orbitals. These ligand contributions are responsible for that the rotatory strength being nonzero. The mechanism by which formally forbidden d−d transitions gain their CD intensity has been illustrated in the earlier publications of this series.[46,64] The similar feature in the spectrum of the corresponding bipyridyl complex labeled x′ (Figure 5) is ascribed to the mixing of d−d transitions with MLCT and indicated as x in the simulated spectrum. In the ruthenium and osmium complexes, such d−d transitions take place as expected at much higher energies and are likely hidden by more intense internal ligand transitions.

4. Origin of the CD in Tris(bipyridyl) and Similar Complexes

We have shown in the previous section that the low-energy part of the CD spectra for the tris(bipyridyl) complexes of the iron group metals is ascribed to the MLCT excitations and the high-energy part to the internal ligand $\pi \rightarrow \pi^*$ transitions. The origin of the CD associated with MLCT excitations, in general, has been addressed within a qualitative framework developed elsewhere[46] and will not be discussed again here. We shall as a consequence in this section focus on the mechanism that gives rise to the CD for the internal ligand transitions. To this end, we first consider the individual $\pi \rightarrow \pi^*$ transitions on the free ligands.

4.1. Electric and Magnetic Allowed $\pi \rightarrow \pi^*$ Transitions in the Individual bpy Molecules. In a single planar π-conjugated molecule, e.g., 2,2′-bipyridine, electric transition dipole moments of the $\pi \rightarrow \pi^*$ excitations are polarized in the molecular plane and will be directed either along the long axis (y') or the short axis (z'), as shown in Figure 2. The prime is used to distinguish the local coordinate system for the free ligands from the global one for the complexes. It is noted that the long-axis-polarized transitions involve ligand MOs belonging to different symmetries, that is, $a_2 \rightarrow b_1$, while the short-axis-polarized transitions occur between orbitals of the same representation, that is, $a_2 \rightarrow a_2$ or $b_1 \rightarrow b_1$. On the other hand, the $a_2 \rightarrow b_1$ transitions are associated with a magnetic transition moment that is polarized perpendicular to the molecular plane along the x' axis of Figure 2. It is then obvious that the $\pi \rightarrow \pi^*$ transitions in individual bpy molecules are optically inactive because the associated electric and magnetic transition dipoles are perpendicular to each other.

In complexes $[M(L-L)_3]^{n+}$ where the coordination of three ligands leads to a D_3 environment, the coupling between the transition moments on individual ligands might give rise to nonvanishing CD. The CD can be accounted for by contributions to the rotatory strengths from individual transition moments as shown below.

4.2. Symmetry-Adapted Microstates Responsible for the Exciton CD Bands in the $[M(bpy)_3]^{2+}$ Complexes. It follows from Tables 1−3 and Figure 1 that the major contributions to the exciton transitions in $[M(bpy)_3]^{2+}$ are due to one-electron excitations from the occupied Lπ-based orbitals $2a_1$ and 4e to the virtual Lπ^* levels $4a_2$ and 6e. The L$\pi \rightarrow$ Lπ^* transitions give rise to a number of symmetry-adapted microstates, as illustrated in Table 4. Because in this case the MOs $4e-2a_1$ and $6e-4a_2$ involved in the excitations are largely made up of free ligand orbitals $2a_2$ and $1b_1$ (Figure 2), respectively, the rotatory strengths are primarily determined by $\langle 2a_2|\mu_{y'}|1b_1\rangle$ and $\langle 1b_1|m_{x'}|2a_2\rangle$ on individual ligands with a given molecular structure of the complex. It is noted that the transition moments on the ligands are all symmetry-related and can be expressed in terms of the transition moments on one ligand. In doing so, the effect of moving the origin of the magnetic transition dipole operator from the metal center to the center of the ligand has been neglected without changing the qualitative picture of the model. We can then readily obtain the transition moments and rotatory strengths associated with transitions from the ground state to the microstates (see Table 4 and Figure 6). In the table, the coefficients of the symmetry ligand π orbitals are omitted by further assuming that all of the MOs involved are purely made of the ligand orbitals. For a free bipyridyl ligand shown in Figure 2, $\langle 2a_2|\mu_{y'}|1b_1\rangle$ and $\langle 1b_1|l_{x'}|2a_2\rangle$ are computed to be 2.397 and −0.2394, respectively, in atomic units with $\hat{\boldsymbol{\mu}} = \vec{\mathbf{r}}$ and $\hat{\mathbf{l}} = 2c\hat{\mathbf{m}}$. It then follows from Table 4 that, in the Λ configuration of $[M(bpy)_3]^{2+}$ with $0 < \omega < 90°$, the rotatory strength of the E transitions is positive while that of the A_2 transitions is negative.

4.3. Origin of the Rotatory Strengths of the Transitions Involved in the Exciton CD Bands. We note that excited states might, in practice, be expressed as a linear combination of microstates having the same symmetry:

$$\Psi_\lambda = \sum_i C_i \Phi_i \tag{1}$$

The rotatory strength will therefore depend also on the coefficients that mix symmetry-adapted microstates.

$A_1 \rightarrow A_2$ Transition. The overall A_2 excited-state wave function can in accordance with Table 4 be written as

$$\Psi_{A_2} = C_1 \Phi_{1A_2} + C_2 \Phi_{2A_2} \tag{2}$$

We then have

$$R_{A_2} = \mathrm{Im}\langle A_1|\hat{\boldsymbol{\mu}}|A_2\rangle \cdot \langle A_2|\hat{\mathbf{m}}|A_1\rangle = -\mathscr{R}(C_1 + \sqrt{2}C_2)^2 \tag{3}$$

(64) Fan, J.; Ziegler, T. *Chirality* **2008**, *20*, 938–950.

Table 4. Transition Moments and Rotatory Strengths Associated with $\pi \rightarrow \pi^*$ Transitions from the Ground State to Excited Microstates in $[M(bpy)_3]^{2+}$

microstates[a]		wave functions[b,c]	$\langle 0\|\hat{\boldsymbol{\mu}}\|\lambda\rangle$[d,e,f]	$\langle\lambda\|\hat{\mathbf{m}}\|0\rangle$[f,g,h]	R^i
$1A_2$		$\frac{1}{\sqrt{2}}(\|2a_1 4\bar{a}_2\| - \|2\bar{a}_1 4a_2\|)$	$\sqrt{2}\mu_{y'}\cos\omega$	$\sqrt{2}m_{x'}\sin\omega$	$2\mu_{y'}m_{x'}\sin\omega\cos\omega$
$2A_2$		$\frac{1}{2}(\|4e_y 6\bar{e}_x\| - \|4\bar{e}_y 6e_x\| - \|4e_x 6\bar{e}_y\| + \|4\bar{e}_x 6e_y\|)$	$2\mu_{y'}\cos\omega$	$2m_{x'}\sin\omega$	$4\mu_{y'}m_{x'}\sin\omega\cos\omega$
1E	$1E_x$	$\frac{1}{\sqrt{2}}(\|4e_y 4\bar{a}_2\| - \|4\bar{e}_y 4a_2\|)$	$-\mu_{y'}\sin\omega$	$m_{x'}\cos\omega$	$-\mu_{y'}m_{x'}\sin\omega\cos\omega$
	$1E_y$	$\frac{1}{\sqrt{2}}(\|4e_x 4\bar{a}_2\| - \|4\bar{e}_x 4a_2\|)$	$\mu_{y'}\sin\omega$	$-m_{x'}\cos\omega$	$-\mu_{y'}m_{x'}\sin\omega\cos\omega$
2E	$2E_x$	$\frac{1}{2}(\|4e_x 6\bar{e}_x\| - \|4\bar{e}_x 6e_x\| - \|4e_y 6\bar{e}_y\| + \|4\bar{e}_y 6e_y\|)$	$-\mu_{y'}\sin\omega$	$m_{x'}\cos\omega$	$-\mu_{y'}m_{x'}\sin\omega\cos\omega$
	$2E_y$	$\frac{1}{2}(\|4e_x 6\bar{e}_y\| - \|4\bar{e}_x 6e_y\| + \|4e_y 6\bar{e}_x\| - \|4\bar{e}_y 6e_x\|)$	$\mu_{y'}\sin\omega$	$-m_{x'}\cos\omega$	$-\mu_{y'}m_{x'}\sin\omega\cos\omega$
3E	$3E_x$	$\frac{1}{\sqrt{2}}(\|2a_1 6\bar{e}_x\| - \|2\bar{a}_1 6e_x\|)$	$-\mu_{y'}\sin\omega$	$m_{x'}\cos\omega$	$-\mu_{y'}m_{x'}\sin\omega\cos\omega$
	$3E_y$	$\frac{1}{\sqrt{2}}(\|2a_1 6\bar{e}_y\| - \|2\bar{a}_1 6e_y\|)$	$-\mu_{y'}\sin\omega$	$m_{x'}\cos\omega$	$-\mu_{y'}m_{x'}\sin\omega\cos\omega$
A_1(GS)		$\|3a_1\ 3\bar{a}_1\ 5e_x\ 5\bar{e}_x\ 5e_y\ 5\bar{e}_y\|$			

[a] One-electron excitations involving open shells give rise to a number of (micro)states that are described by a symmetry-determined linear combination of determinants. [b] Refer to Figure 1 for one-electron MOs. [c] A one-electron transition $\psi_i\alpha \rightarrow \psi_j\alpha$ is represented by the Slater determinant $|\bar{\psi}_i\psi_j|$ where all of the other occupied ground-state orbitals are omitted. In the same way, $\psi_i\beta \rightarrow \psi_j\beta$ is represented by $|\psi_i\bar{\psi}_j|$. [d] Electric transition dipole moment for transition to a microstate. [e] $\mu_{y'} = \langle 2a_2|\mu_{y'}|1b_1\rangle$. [f] Refer to Figure 2 for single ligand orbitals $2a_2$ and $1b_1$. [g] Magnetic transition dipole moment for transition to a microstate. [h] $m_{x'} = \langle 1b_1|m_{x'}|2a_2\rangle$. [i] Rotatory strength for transition to a microstate.

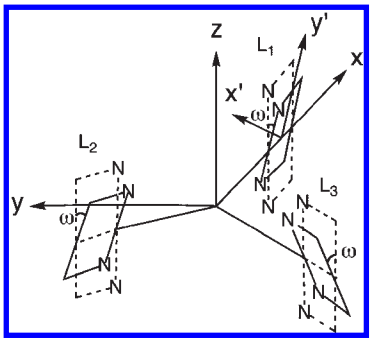

Figure 6. Orientations of electric and magnetic transition dipole moments associated with the long-axis-polarized $\pi \rightarrow \pi^*$ excitations in free ligand.

with $\mathscr{R} = -2\mu_{y'}m_{x'}\sin\omega\cos\omega$. The in-phase combination of the two microstates with $C_1 = \sqrt{1/3}$ and $C_2 = \sqrt{2/3}$ in an ideal case gives rise to $R_{A_2} = -3\mathscr{R}$, which has a negative magnitude for the Λ configuration. The out-of-phase combination with $C_1 = \sqrt{2/3}$ and $C_2 = -\sqrt{1/3}$ gives rise to a zero rotatory strength. For Λ-$[Os(bpy)_3]^{2+}$, C_1:C_2 is found to be 0.4139:0.6470 from a TD-DFT calculation using the Tamm−Dancoff approximation (TDA).[65] This corresponds to excitation no. 8 of Table 1. The rotatory strength associated with the out-of-phase combination is considerably weaker and is not indicated in the simulated CD spectrum.

$A_1 \rightarrow E$ Transition. Likewise, we have the wave function for the E transition

$$\Psi_E = C_1\Phi_{1E} + C_2\Phi_{2E} + C_3\Phi_{3E} \quad (4)$$

and the rotatory strength for the E_x component

$$R_{E_x} = \frac{1}{2}\mathscr{R}(C_1 + C_2 + C_3)^2 \quad (5)$$

with $\mathscr{R}$ being the same quantity as defined in eq 3. The rotatory strength for the E_y component has the same magnitude as that of E_x in spite of the different MOs involved. The E transition achieves a rotatory strength of $3\mathscr{R}$ (positive for the Λ configuration) from the in-phase combination of the microstates 1E, 2E, and 3E with $C_1 = C_2 = C_3 = 1/\sqrt{3}$ in an ideal case. On the other hand, the rotatory strengths would vanish in the theory for the two out-of-phase combinations. In the real situation of Λ-$[Os(bpy)_3]^{2+}$, a TDA calculation found the in-phase combination with C_1:C_2:C_3 = 0.3633:0.4552:0.4936, which corresponds to excitation no. 7 of Table 1. Again, the CD intensity associated with the out-of-phase combinations is particularly small and is not indicated in the spectrum.

The sign and qualitative intensity of the exciton CD in $[M(phen)_3]^{2+}$ can be interpreted in a similar way. In this case, the important transition moments in a free phen ligand (see Figure S4 in the Supporting Information) involve $\langle 1a_2|\mu_{y'}|2b_1\rangle$ (2.0722) and $\langle 2b_1|l_{x'}|1a_2\rangle$ (−0.8915). The coefficients that combine different symmetry-adapted microstates vary in absolute value.

4.4. Energy Splitting of the A_2 and E Exciton CD Bands. It is readily seen from Table 4 that the overall sum of the rotatory strengths due to the A_2 and E transitions canceled out, as is expected from the theoretical sum rule.[66,67] Therefore, no CD should be observed if the A_2 and E transitions occur at the same energy. This is certainly not the case in the actual situation where transitions to excited states of A_2 and E symmetry take place at different energies (Tables 1−3).

Within the TD-DFT formalism, we ascribe the splitting between states A_2 and E giving rise to exciton transitions as being mainly due to the energy difference of the MOs involved in the one-electron excitations. The orbital energy differences are, in turn, caused by interactions between the π-ligand orbitals and the d set on the metal center as discussed in section 3. We expect, in addition, the splitting to be influenced by overlaps between orbitals on different ligands. For symmetry-adapted microstates $2A_2$ and 2E, which both arise from the one-electron excitation 4e → 6e, two-electron Coulomb integrals are responsible for the splitting.

On the basis of the orbital energy order in Figure 1, the symmetry-adapted microstates are qualitatively predicted to have the energy order $1E(4e \rightarrow 4a_2) < 1A_2(2a_1 \rightarrow 4a_2) < 2E(4e \rightarrow 6e) < 3E(2a_1 \rightarrow 6e) < 1A_2(4e \rightarrow 6e)$, as illustrated in Figure 7. The energy order is due to the

(65) Hirata, S.; Head-Gordon, M. *Chem. Phys. Lett.* **1999**, *314*, 291–299.
(66) Condon, E. U. *Rev. Mod. Phys.* **1937**, *9*, 432–457.
(67) Sugano, S. *J. Chem. Phys.* **1960**, *33*, 1883–1884.

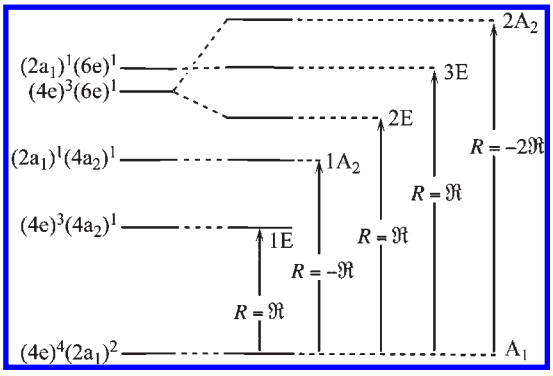

Figure 7. Schematic microstate splitting for $4e \rightarrow 4a_2$, $2a_1 \rightarrow 4a_2$, $4e \rightarrow 6e$, and $2a_1 \rightarrow 6e$ one-electron excitations in $[M(bpy)_3]^{2+}$. $\mathcal{R} = -2\mu_y m_{x'} \sin \omega \cos \omega$.

fact that the 4e and $2a_1$ orbitals are almost degenerate (see Figure 1). We note that the A_1 microstate arising from the $4e \rightarrow 6e$ excitation has been omitted from Figure 7 because it is both electrically and magnetically forbidden. In real situations where the overall A_2 and E states are the combinations of symmetry-adapted microstates, the energies then rely on contributions from different one-electron excitations. From the spectral information compiled in Tables 1−3 as well as the coefficients from the TDA calculations presented earlier in section 4.3, we see that the A_2 exciton state has a major involvement of the microstate $2A_2$, which has the highest excitation energy among the five counterparts (Figure 7). Meanwhile, for the E state, in most cases contributions from the three microstates are comparable. We thus expect an energy order of $v(E) < v(A_2)$ for the overall A_2 and E exciton states, which is in line with the results obtained from TD-DFT calculations.

Even though part of the argument made above is based on the MO information of the bpy complexes, it is generally applicable to the phen complexes and other analogues that exhibit similar electronic structures.

Historically, the LC $\pi \rightarrow \pi^*$ transitions have been treated by the classic exciton theory.[8,10,11] We present in Supporting Information the relationship between our model and the classic theory.

5. Conclusion

Electronic structures and CD spectra of bpy and phen complexes of iron group metals have been studied using the TD-DFT method. The spectroscopic properties of the complexes are closely related to their electronic structures. From the DFT calculations, the most important frontier orbitals involved in the absorption region investigated include the ligand-based π HOMO−1's ($2a_1$ and 4e), the metal-based HOMO's (5e and $3a_1$), and the ligand-based π^* LUMO's ($4a_2$ and 6e) for the bpy complexes. In the case of phen complexes, the orbitals of the same key are the HOMO−2's ($1a_1$ and 3e), the HOMO's (5e and $2a_1$), and the LUMO's ($4a_2$ and 6e). The trigonal splitting of these orbitals in the D_3 environment is elucidated in terms of the metal−ligand orbital interaction based on symmetry arguments and the overlap expressions derived earlier. These interactions give rise to an increment of the trigonal splitting of the π^* LUMOs in going from iron to osmium as a result of increasing orbital overlaps.

As was just mentioned, the occupied metal d orbitals (t_g set) are situated between the ligand π and π^* orbitals on the energy scale in all of the complexes studied. Accordingly, the lowest-energy region of the CD spectra appears to result from the MLCT transitions, in line with the experimental assignment. This finding is, however, in contrast to the earlier prediction from Hückel calculations for the iron system in which the LUMOs appear to be the metal-based e_g set and the first band of the absorption spectrum was assigned to the d−d transitions. The higher-energy region of the spectra is found to derive from the LC excitations. The two most intense CD bands, also referred to as exciton CD bands, show opposite signs, with the positive one occurring at lower energy for the complex ion of the Λ configuration. The high intensity of these bands is ascribed to the long-axis-polarized $\pi \rightarrow \pi^*$ excitations localized on the ligands. The sign pattern of the two exciton bands, in connection with the TD-DFT calculations, is rationalized by the orientation of the transition moments associated with the $\pi \rightarrow \pi^*$ excitations on the individual ligands. It was further found that the energy difference of the ligand orbitals, in particular the π^* LUMOs, is responsible for the trigonal splitting of the two exciton bands. The orbital energy difference is, in turn, due to both metal−ligand and interligand bonding.

Tris(bipyridyl) metal complexes continue to play a significant role in inorganic photochemistry. We have here provided the first modern computational study on the CD of $[M(bpy)_3]^{2+}$ (M = Fe, Ru, Os) based on TD-DFT. Our study affords a full analysis of the CD due to d−d and metal-to-ligand transitions as well as the LC exciton excitations. Further studies on the optical rotatory dispersion of $[M(bpy)_3]^{2+}$ (M = Fe, Ru, Os) and related complexes will be reported in a separate account,[68] where we will also consider the d−d transition region for iron complexes described by different functionals.

Acknowledgment. This work has received financial support from the National Science and Engineering Research Council of Canada. J.F. acknowledges financial support of the Alberta Ingenuity Fund. J.A. is grateful for financial support of his research by the National Science Foundation (Grant CHEM 0447321). T.Z. thanks the Canadian Government for a Canada Research Chair.

Supporting Information Available: Discussion of the relationship between the current DFT model and the classic exciton model, definition of symmetrized metal d orbitals and ligand σ/π orbitals in D_3 symmetry, frontier MOs in phen, and molecular level diagrams, simulated CD spectra, and detailed spectral information for $[M(phen)_3]^{2+}$ (M = Fe, Ru, Os). This material is available free of charge via the Internet at http://pubs.acs.org.

(68) Rudolph, M.; Autschbach, J. to be submitted.